A Link Between Childhood Adversity and Trait Anger Reflects Relative Activity of the Amygdala and Dorsolateral Prefrontal Cortex

Supplemental Information

Supplemental Methods

dlPFC Paradigm

The paradigm included 10 trials for each of 6 different conditions, including 3 control conditions, consisting only of a 3 s response phase, and 3 working memory (WM) conditions, consisting of a 0.5 s encoding phase followed by a 4 s maintenance interval and a 3 s response phase (Supplemental Fig. S1; for details, see Fig.1 in (1)). Control and WM conditions were interleaved with jittered rest intervals lasting 4-8.5 s for a total scan length of 708 s. Responses were recorded via an MR-compatible button box using the index (left button) and middle (right button) fingers of the dominant hand.

During the control conditions, participants performed 1) a simple motor task (M) in which they pressed either the left or the right button according to a prompt, 2) a numerical size judgment task (J) in which they chose the number on the left or right based on an instruction to choose either the larger or the smaller number, and 3) a numerical computation and size judgment task (CJ) in which they performed a numerical subtraction of 2 or 3 from either the left or right number, and made a numerical size judgment as instructed.

In the first WM condition, participants viewed 2 numbers during the brief encoding phase, then recalled the numbers and performed a numerical size judgment as instructed (E_RJ). In the second WM condition, the participants additionally performed subtraction of 2 or 3 from

one of the remembered numbers as indicated before making the numerical size judgment during recall (E_RCJ). In the final WM condition, participants performed subtraction of 2 or 3 from one of the 2 numbers during the brief encoding phase, then recalled the resulting two numbers and performed a numerical size judgment as instructed during the response phase after the maintenance interval (EC_RJ). In each WM condition trial, all the numbers were single digits from 0 to 9; the two numbers on which the numerical size judgment was ultimately performed (after numerical computation if applicable) were equally balanced across 0 to 9, and equally likely to differ by either 1 or 3 units.

fMRI Data Acquisition

Each participant was scanned using one of the two identical research-dedicated GE MR750 3T scanner equipped with high-power high-duty-cycle 50-mT/m gradients at 200 T/m/s slew rate, and an eight-channel head coil for parallel imaging at high bandwidth up to 1MHz at the Duke-UNC Brain Imaging and Analysis Center. A semi-automated high-order shimming program was used to ensure global field homogeneity. A series of 34 interleaved axial functional slices aligned with the anterior commissure-posterior commissure plane were acquired for full-brain coverage using an inverse-spiral pulse sequence to reduce susceptibility artifacts (TR/TE/flip angle=2000 ms/30 ms/60; FOV=240mm; 3.75×3.75×4mm voxels; interslice skip=0). Four initial radiofrequency excitations were performed (and discarded) to achieve steady-state equilibrium. To allow for spatial registration of each participant's data to a standard coordinate system, high-resolution three-dimensional T1-weighted structural images were obtained in 162 axial slices using a 3D Ax FSPGR BRAVO sequence (TR/TE/flip angle = 8.148 ms / 3.22 ms / 12°; voxel size=0.9375x0.9375x1mm; FOV=240mm; interslice skip=0; total scan time = 4 min

and 13 s). In addition, high-resolution structural images were acquired in 34 axial slices coplanar with the functional scans and used for spatial registration for participants without Ax FSPGR BRAVO images (TR/TE/flip angle=7.7 s/3.0 ms/12; voxel size=0.9×0.9×4mm; FOV=240mm, interslice skip=0).

fMRI Data Preprocessing

Anatomical images for each subject were skull-stripped, intensity-normalized, and nonlinearly warped to a study-specific average template in the standard stereotactic space of the Montreal Neurological Institute template using ANTs (2). BOLD time series for each subject were processed in AFNI (3). Images for each subject were despiked, slice time-corrected, realigned to the first volume in the time series to correct for head motion, coregistered to the anatomical image using FSL's Boundary Based Registration (4), spatially normalized into MNI space using the non-linear warp from the anatomical image, resampled to 2 mm isotropic voxels, and smoothed to minimize noise and residual difference in gyral anatomy with a Gaussian filter, set at 6-mm full-width at half-maximum. All transformations were concatenated so that a single interpolation was performed. Voxel-wise signal intensities were scaled to yield a time series mean of 100 for each voxel. Volumes exceeding 0.5 mm framewise displacement or 2.5 standardized DVARS (temporal derivative of RMS variance over voxels) (5,6) were censored from the GLM.

fMRI Quality Assurance Criteria

Quality control criteria for inclusion of a participant's imaging data were: > 5 volumes for each condition of interest retained after censoring for FD and DVARS and sufficient temporal SNR

within the bilateral amygdala, defined as greater than 3 standard deviations below the mean of this value across subjects. The amygdala was defined using a high-resolution template generated from 168 Human Connectome Project datasets (7). Additionally, data were only included in further analyses if the participant demonstrated sufficient engagement with the task, defined as achieving at least 75% accuracy during the face matching condition.

Quality control criteria for inclusion of a participant's imaging data were: < 5% volumes exceed artifact detection criteria for motion or signal intensity outliers and ≥ 90% coverage of signal within 5 mm bilateral dlPFC spheres centered at (±42, 16, 36). Additionally, data were only included in further analyses if the participant demonstrated sufficient engagement with the task, defined as at least 75% average accuracy across all trial types, and at least 50% accuracy within each trial type.

Supplemental Results

Moderation Analyses with CTQ and STAXI Subscales

For completeness, moderation analyses were repeated using the CTQ and STAXI subscales. As there were 5 subscales for the CTQ and 2 subscales for the STAXI, there were a total of 18 possible combinations of CTQ-STAXI scores including the total scores. Among them, the following two pairs were significant after correcting for multiple comparisons (Bonferroni corrected $p < 0.05$): CTQ Emotional Abuse–STAXI total ($b = 5.11$, 95% confidence interval (CI) = [2.31, 7.9], $\Delta R^2 = 0.04$, $p = 0.0004$) and CTQ Emotional Abuse–STAXI Anger Temperament ($b = 2.18$, 95% CI = [0.98, 3.39], $\Delta R^2 = 0.04$, $p = 0.0004$).

Supplemental Figure

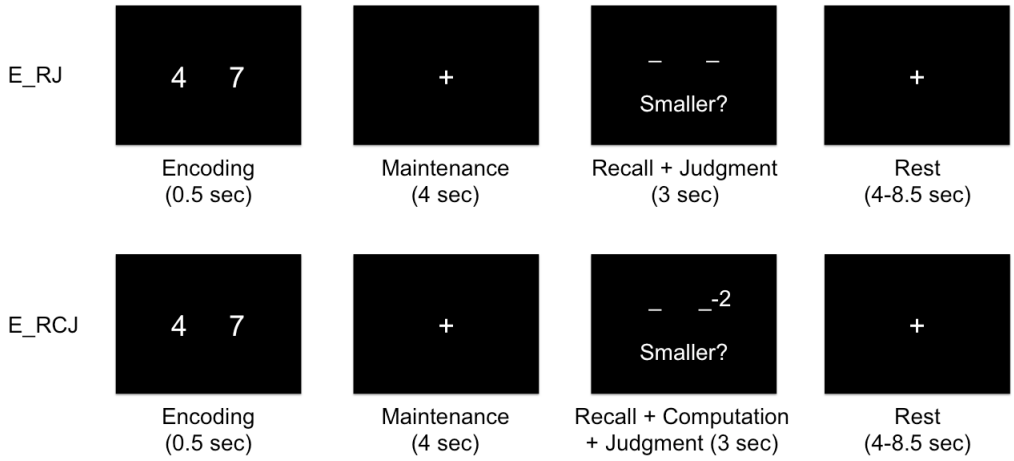

Supplemental Fig. S1. Sample trials for the E_RJ and E_RCJ conditions. E_RCJ > E_RJ contrast was used to isolate the computational component of working memory.

Supplemental Table

Supplemental Table S1. Conditional effects of childhood adversity on trait anger at low, intermediate, and high activity of the dlPFC and amygdala.

dlPFC	Amygdala	*b* (SE)	*t*	*p*
Low	Low	0.30 (0.07)	4.05	0.001
Low	Intermediate	0.29 (0.06)	4.72	< 0.0001
Low	High	0.28 (0.07)	3.82	0.002
Intermediate	Low	0.15 (0.04)	3.41	0.008
Intermediate	Intermediate	0.21 (0.04)	5.74	< 0.0001
Intermediate	High	0.28 (0.05)	6.12	< 0.0001
High	Low	0.001 (0.06)	0.01	0.994
High	Intermediate	0.14 (0.04)	3.52	0.005
High	High	0.28 (0.05)	6.33	< 0.0001

Note: Low, intermediate, and high was defined as < -1 standard deviation (SD), -1 SD < and < +1 SD, and > +1 SD, respectively. dlPFC: dorsolateral prefrontal cortex; SE: standard error.

Supplemental References

1. Scult MA, Knodt AR, Swartz JR, Brigidi BD, Hariri AR (2017): Thinking and feeling: Individual differences in habitual emotion regulation and stress-related mood are associated with prefrontal executive control. *Clin Psychol Sci,* 5: 150-157.
2. Klein A, Andersson J, Ardekani BA, Ashburner J, Avants B, Chiang M-C, *et al.* (2009): Evaluation of 14 nonlinear deformation algorithms applied to human brain MRI registration. *Neuroimage,* 46: 786-802.
3. Cox RW (1996): AFNI: software for analysis and visualization of functional magnetic resonance neuroimages. *Comput Biomed Res,* 29: 162-173.
4. Greve DN, Fischl B (2009): Accurate and robust brain image alignment using boundary-based registration. *Neuroimage,* 48: 63-72.
5. Nichols TE (2017): Notes on creating a standardized version of DVARS. *arXiv preprint,* arXiv:170401469.
6. Power JD, Mitra A, Laumann TO, Snyder AZ, Schlaggar BL, Petersen SE (2014): Methods to detect, characterize, and remove motion artifact in resting state fMRI. *Neuroimage,* 84: 320-341.
7. Tyszka JM, Pauli WM (2016): *In vivo* delineation of subdivisions of the human amygdaloid complex in a high-resolution group template. *Hum Brain Mapp,* 37: 3979-3998.